Available online at www.sciencedirect.com
SCIENCE DIRECT®
Journal of Computational Physics 187 (2003) 639–659
JOURNAL OF COMPUTATIONAL PHYSICS
www.elsevier.com/locate/jcp

A fast solver of the shallow water equations on a sphere using a combined compact difference scheme

Tomonori Nihei *, Katsuya Ishii [1]

Department of Computational Science and Engineering, Nagoya University, Nagoya, Japan

Received 31 January 2002; received in revised form 10 October 2002; accepted 24 February 2003

Abstract

The spectral-like three-point combined compact difference (sp-CCD) scheme is developed for the shallow water models on a sphere, which is originally proposed by Chu and Fan (J. Comput. Phys. 140 (1998) 370). A standard test set proposed by Williamson et al. (J. Comput. Phys. 102 (1992) 211) is used to evaluate the accuracy of the new method. It is shown that the accuracy of the method is comparable to that of the spherical harmonics model as a whole. The relative efficiency of the method with respect to the spherical harmonics model appears from the resolution of 512×256, and it becomes significant for the higher resolutions. The test results suggest that the method could be extended to numerical atmospheric models.

AMS: 65; 76; 86

Keywords: Combined compact difference; Shallow water equations; Compact filter; Weather prediction

1. Introduction

Recent analyses suggest that highly precise and effective computational methods are required for the global climate models [19]. The spherical transform method is widely used for its accuracy, but its computational cost is rapidly larger in the calculation with higher grid resolution. For example, the cost for two-dimensional problem on a sphere is proportional to N^3, where N is the number of grid points in the latitude direction.

Various methods have been proposed as alternative methods to the current spectral transform method. Williamson et al. [19] proposed the standard suit of test cases to the shallow water equations

* Corresponding author.
E-mail addresses: nihei@fluid.cse.nagoya-u.ac.jp (T. Nihei), ishii@itc.nagoya-u.ac.jp (K. Ishii).
[1] Present address: Information Technology Center, Nagoya University, Nagoya, Japan, 464-8601.

0021-9991/03/$ - see front matter
doi:10.1016/S0021-9991(03)00152-9

in spherical geometry in the aid of the search for promising methods. Merilees [14] and Fornberg [5] proposed pseudospectral method utilizing double Fourier series to compute the spatial derivatives on latitude–longitude grids. They applied it to the shallow water equations on the sphere. Cheong [2,3] proposed a spectral method using double Fourier series as basis functions, and evaluated the solutions of all Williamson's test cases. These pseudospectral and spectral methods utilizing double Fourier series realize high accuracy and a reduction of computational cost by using the FFT method instead of the associated Legendre transforms. Finite difference methods, which are widely used in the various fluid simulations, are also investigated since their computational cost is small. In the problem mentioned above, the cost of finite difference methods is proportional to N^2 while that of the double Fourier methods is proportional to $N^2 \log N$. Spotz et al. [17] examined a fourth-order three-point compact difference scheme with a spectral spatial filter for Williamson's test cases, and concluded that the accuracy of their method is comparable to the spectral transform method based on the spherical harmonics for all seven test cases. When we consider the global models with longitude–latitude grids, additional treatment is required to avoid the 'polar problem' due to the concentration of grid points near the poles. Filtering schemes are used in the above three methods so that small scales are diminished near the poles. Rančić et al. [15] used a finite difference scheme on the grid geometry of the expanded spherical cube, applied it to a global shallow water model, and showed that the model works without polar filter. The finite volume scheme is also investigated by Lin and Rood [11]. They proposed a global shallow water model based on the flux form semi-Lagrangian scheme and calculated two cases of the Williamson's standard test cases. They concluded that the scheme is competitive in accuracy.

Compact difference (CD) schemes, which were introduced in the 1930s, have shown its accuracy for the small scales significantly higher than traditional schemes with the same stencil size. Lele [10] generalized the idea on compact schemes and suggested that the resolution, which means the accuracy in Fourier space, should be considered in addition to the formal accuracy. He also proposed spectral-like compact difference schemes and compact schemes for interpolation and filtering. Many compact schemes are proposed and used in different flow calculations [1,6,9,13]. It is noted that Spotz et al. [17] used a fourth order compact scheme, but their filter is a spectral scheme. In 1998, Chu and Fan [4] proposed a three-point combined compact difference (CCD) scheme that uses a combined derivative formulation, and showed that it has an improved spectral resolution with a cost which is comparable to that of the standard compact scheme. A similar class of schemes was also studied by Mahesh [12] and referred as the coupled-derivative or C–D schemes.

In this paper, we attempt to derive a combined compact difference scheme with spectral-like resolution, and evaluate its performance using the test cases for the shallow water equations in spherical geometry proposed by Williamson et al. We use a compact scheme for spatial filter that is proposed by Lele [10]. This paper is organized as follows. Section 2 describes the CCD scheme with spectral-like resolution derived in this study. The governing equations of the Williamson's standard test suite that are used for performance measurements and our solution method including a spatial filtering scheme are explained in Section 3. Section 4 presents the results of the test cases. Discussions and conclusions are drawn in Section 5.

2. A CCD scheme with spectral-like resolution

Consider a uniform grid with spacing Δx and the value of a function $f(x)$ at ith grid point x_i is given by $f_i \equiv f(x_i)$. In CCD schemes, the derivatives of the function at a grid point are approximated by using them and the value of the function and its derivatives at the neighboring points. Chu and Fan [4] proposed a sixth-order and eighth-order scheme. The eighth-order scheme can be written as

$$f_i' + a_1\left(f_{i+1}' + f_{i-1}'\right) + b_1\Delta x\left(f_{i+1}'' - f_{i-1}''\right) + c_1(\Delta x)^2\left(f_{i+1}''' + f_{i-1}'''\right) = \frac{d_1}{\Delta x}(f_{i+1} - f_{i-1}), \tag{2.1}$$

$$f_i'' + \frac{a_2}{\Delta x}\left(f_{i+1}' - f_{i-1}'\right) + b_2\left(f_{i+1}'' + f_{i-1}''\right) + c_2\Delta x\left(f_{i+1}''' - f_{i-1}'''\right) = \frac{d_2}{(\Delta x)^2}(f_{i+1} - 2f_i + f_{i-1}), \tag{2.2}$$

$$f_i''' + \frac{a_3}{(\Delta x)^2}\left(f_{i+1}' + f_{i-1}'\right) + \frac{b_3}{\Delta x}\left(f_{i+1}'' - f_{i-1}''\right) + c_3\left(f_{i+1}''' + f_{i-1}'''\right) = \frac{d_3}{(\Delta x)^3}(f_{i+1} - f_{i-1}). \tag{2.3}$$

where 12 parameters of a_k, b_k, c_k, d_k $(k = 1, 2, 3)$ are given as

$$a_1 = \frac{19}{32}, \quad b_1 = -\frac{1}{8}, \quad c_1 = \frac{1}{96}, \quad d_1 = \frac{35}{32}, \tag{2.4}$$

$$a_2 = \frac{29}{16}, \quad b_2 = -\frac{5}{16}, \quad c_2 = \frac{1}{48}, \quad d_2 = 4, \tag{2.5}$$

$$a_3 = -\frac{105}{16}, \quad b_3 = \frac{15}{8}, \quad c_3 = -\frac{3}{16}, \quad d_3 = -\frac{105}{16}. \tag{2.6}$$

These parameters are determined by minimizing the truncation errors of (2.1)–(2.3). In this case, the formal accuracies of (2.1)–(2.3) become eighth-order, eighth-order, and sixth-order, respectively. Lele pointed out that the resolution of the scheme is also important. To evaluate the resolution characteristics of the scheme, Fourier analysis is commonly used. The function can be approximated by the following Fourier series as:

$$f(x) = \sum_{k=-N/2}^{N/2} \widehat{f_k}\exp(2\pi \mathrm{i}kx/L), \tag{2.7}$$

where $\mathrm{i} = \sqrt{-1}$ and L is the length of the domain and N is the number of grid points, respectively. One Fourier mode can be written as $f_k = \widehat{f_k}\exp(\mathrm{i}ws)$ where $w = 2\pi k\Delta x/L$ is the scaled wavenumber and $s = x/\Delta x$ is the scaled coordinate, where $\Delta x = L/N$ and $w < \pi$.

The derivative of f_k is

$$\frac{\mathrm{d}}{\mathrm{d}x}f_k = \frac{\mathrm{i}w}{\Delta x}f_k. \tag{2.8}$$

However, we obtain in finite difference approximation,

$$\frac{\delta}{\delta x}f_k = \frac{\mathrm{i}w'}{\Delta x}f_k, \tag{2.9}$$

where w' is a function of w and is called the modified wavenumber. The modified wavenumber shows the resolution characteristics of the scheme. A difference scheme is considered to be capable of resolving waves in the range of wavenumber $w < W$ well when the relative error $e(w)$ satisfies

$$e(w) = \frac{|w'(w) - w|}{w} < \epsilon \quad (0 < w < W < \pi), \tag{2.10}$$

where ϵ is a small number. The modified wavenumber of the first derivative $w'(w)$ for this CCD scheme is given by

$$
\begin{aligned}
w'(w) = 2[&\{(1 + b_2c_3 + 3c_2b_3)d_1 + (2b_1 - b_1c_3 + c_1b_3)d_2 - (3b_1c_2 + c_1b_2)d_3\}\sin w \\
&+ \{(b_2 + c_3)d_1 - (b_1 - 2b_1c_3 + 2c_1b_3)d_2 - c_1d_3\}\sin 2w + \{(b_2c_3 - c_2b_3)d_1 \\
&- (b_1c_3 - c_1b_3)d_2 + (b_1c_2 - c_1b_2)d_3\}\sin 3w]/[1 + 2(a_1b_2 + b_1a_2) + 2(a_1c_3 - c_1a_3) \\
&+ 2(b_2c_3 + c_2b_3) + 2\{a_1 + b_2 + c_3 + (a_2c_3 - c_2a_3)b_1 + 3(a_1c_3 - c_1a_3)b_2 + (a_1c_2 - c_1a_2)b_3\} \\
&\times \cos w + 2\{(a_1b_2 - b_1a_2) + (a_1c_3 - c_1a_3) + (b_2c_3 - c_2b_3)\}\cos 2w + 2\{(b_2c_3 - c_2b_3)a_1 \\
&- (b_1c_3 - c_1b_3)a_2 + (b_1c_2 - c_1b_2)a_3\}\cos 3w].
\end{aligned} \tag{2.11}
$$

The modified wavenumber $w'(w)$ and the error $e(w)$ for various schemes are plotted into Figs. 1 and 2, respectively. The exact differentiation is shown as the straight line. CD and CCD schemes have higher resolution than the ordinary central difference schemes. The spectral-like CD scheme has much higher resolution than the other schemes. The slope of the error of $e(w)$ near $w = 0$ in Fig. 2 corresponds to the order of accuracy of the scheme. To research the higher resolution relationship, we relaxed the requirement for formal accuracy of (2.2) and (2.3) by setting the two parameters d_2 and d_3 free. In this case, the other 10 parameters are given as

$$
a_1 = \frac{19}{32}, \quad b_1 = -\frac{1}{8}, \quad c_1 = \frac{1}{96}, \quad d_1 = \frac{35}{32}, \tag{2.12}
$$

$$
a_2 = \frac{11d_2 - 15}{16}, \quad b_2 = -\frac{3d_2 - 7}{16}, \; c_2 = \frac{d_2 - 3}{48}, \tag{2.13}
$$

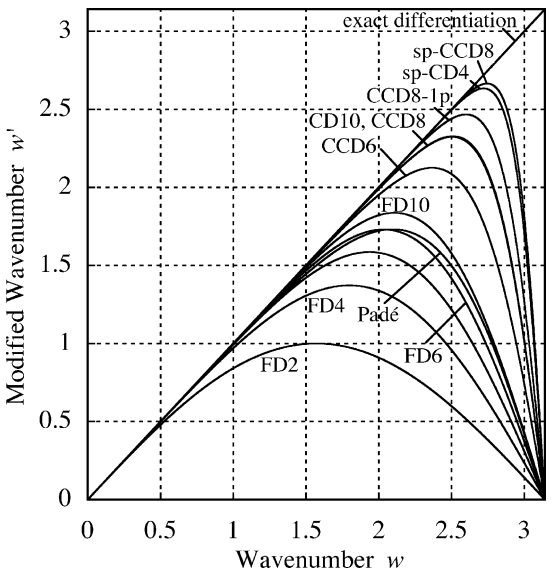

Fig. 1. The modified wavenumber for the first derivative approximations: (FD2) second-order central differences; (FD4) fourth-order central differences; (FD6) sixth-order central differences; (FD8) eighth-order central differences; (FD10) tenth-order central differences; (Padé) standard Padé scheme; (CCD6) sixth-order combined compact difference scheme; (CCD8) eighth-order combined compact difference scheme; (CD10) tenth-order compact difference scheme; (sp-CD4) spectral-like fourth-order compact difference scheme; (CCD8-1p) new eighth-order combined compact difference scheme with fixed d_3; (sp-CCD8) new eighth-order combined compact difference scheme.

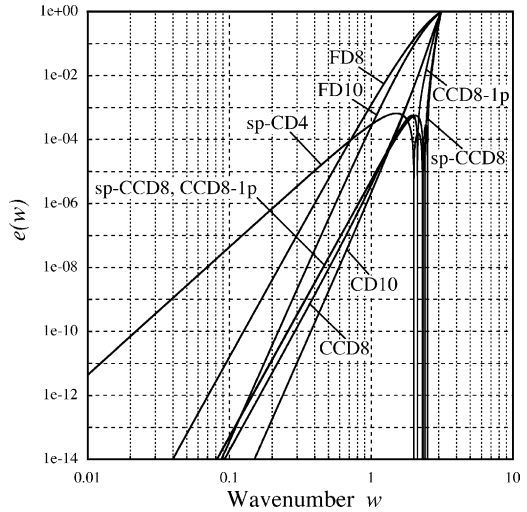

Fig. 2. The error $e(w)$ for the first derivative approximations. For sp-CD4, error was calculated by using the value of α, β, and c in (3.1.6) of [10], and the relationship for a and b in (2.2.8) of [10].

$$a_3 = d_3, \quad b_3 = -\frac{8d_3 + 15}{20}, \quad c_3 = \frac{4d_3 + 15}{60}, \tag{2.14}$$

respectively. In this approximation, the formal accuracy of (2.2) and (2.3) become sixth-order, fourth-order, respectively. The formal accuracy of (2.1) degrades to sixth-order due to using the third-order derivatives with fourth-order accuracy, and the leading order truncation error of (2.1) is proportional to $\Delta x^6 f^{(7)}$. We eliminate this term by using (2.3) which has the leading order truncation error of $O(\Delta x^4 f^{(7)})$. We obtain

$$f'_i + a_1\left(f'_{i+1} + f'_{i-1}\right) + b_1\Delta x\left(f''_{i+1} - f''_{i-1}\right) + c_1(\Delta x)^2\left(f'''_{i+1} - 2f'''_i + f'''_{i-1}\right) = \frac{d_1}{\Delta x}(f_{i+1} - f_{i-1}),$$

$$a_1 = \frac{13}{16}, \quad b_1 = -\frac{3}{16}, \quad c_1 = \frac{1}{60}, \quad d_1 = \frac{21}{16}, \tag{2.15}$$

which has the truncation error of $O(\Delta x^8 f^{(9)})$. By rearranging (2.2), (2.3), and (2.13)–(2.15), we can recover the form of (2.1)–(2.3) with the parameters which are given as

$$a_1 = \frac{8d_3 + 195}{240}, \quad b_1 = -\frac{16d_3 + 255}{1200}, \quad c_1 = \frac{4d_3 + 45}{1800}, \quad d_1 = \frac{8d_3 + 315}{240}, \tag{2.16}$$

$$a_2 = \frac{11d_2 - 15}{16}, \quad b_2 = -\frac{3d_2 - 7}{16}, \quad c_2 = \frac{d_2 - 3}{48}, \tag{2.17}$$

$$a_3 = d_3, \quad b_3 = -\frac{8d_3 + 15}{20}, \quad c_3 = \frac{4d_3 + 15}{60}. \tag{2.18}$$

respectively. Note that in this case the formal accuracy of Eq. (2.1) remains eighth-order. By substituting (2.16)–(2.18) into (2.11), the modified wavenumber can be written as a function of w, d_2, and d_3, that can be written as $w' = w'(w; d_2, d_3)$. These two parameters are used to make the modified wavenumber closer to the exact wavenumber. The two parameters have been determined by minimizing the value of

$$S(d_2, d_3) = \int_0^{w_m} \left(w'(w; d_2, d_3) - w\right)^2 \mathrm{d}w. \tag{2.19}$$

Since $w'(\pi; d_2, d_3) = 0$, the domain near $w = \pi$ should be excluded from integration in (2.19). In this study, w_m is chosen as $w_m = \frac{4}{5}\pi$.

We have obtained values of two parameters as $d_2 = -0.86774$ and $d_3 = -2.1721$. It should be noted that these values might not give the true minimum value of $S(d_2, d_3)$, since there are many local minimums in the numerical approximation of $S(d_2, d_3)$. When d_3 is fixed to $-\frac{105}{16}$, we can find the minimum easily and obtain an eighth-order scheme which third-order derivative is sixth-order accurate. In this case, however, the improvemant of the resolution is not sufficient. As shown in Fig. 1, the modified wavenumber for our CCD scheme almost coincides with that for the spectral-like compact difference scheme proposed by Lele [10]. We call these new class of CCD schemes spectral-like CCD (sp-CCD).

(2.1)–(2.3) can be solved by inverting following the periodic block-tridiagonal system:

$$\begin{pmatrix} \mathbf{B} & \mathbf{C} & \mathbf{O} & \cdots & \cdots & \mathbf{O} & \mathbf{A} \\ \mathbf{A} & \mathbf{B} & \mathbf{C} & \mathbf{O} & & & \mathbf{O} \\ \mathbf{O} & \mathbf{A} & \mathbf{B} & \mathbf{C} & \mathbf{O} & & \vdots \\ \vdots & \ddots & \ddots & \ddots & \ddots & \ddots & \vdots \\ \vdots & & \mathbf{O} & \mathbf{A} & \mathbf{B} & \mathbf{C} & \mathbf{O} \\ \mathbf{O} & & & \mathbf{O} & \mathbf{A} & \mathbf{B} & \mathbf{C} \\ \mathbf{C} & \mathbf{O} & \cdots & \cdots & \mathbf{O} & \mathbf{A} & \mathbf{B} \end{pmatrix} \begin{pmatrix} \mathbf{x}_1 \\ \mathbf{x}_2 \\ \mathbf{x}_3 \\ \vdots \\ \mathbf{x}_{N-2} \\ \mathbf{x}_{N-1} \\ \mathbf{x}_N \end{pmatrix} = \begin{pmatrix} \mathbf{d}_1 \\ \mathbf{d}_2 \\ \mathbf{d}_3 \\ \vdots \\ \mathbf{d}_{N-2} \\ \mathbf{d}_{N-1} \\ \mathbf{d}_N \end{pmatrix}, \tag{2.20}$$

where

$$\mathbf{A} = \begin{pmatrix} a_1 & -b_1\Delta x & c_1(\Delta x)^2 \\ -\frac{a_2}{\Delta x} & b_2 & -c_2\Delta x \\ \frac{a_3}{(\Delta x)^2} & -\frac{b_3}{\Delta x} & c_3 \end{pmatrix}, \quad \mathbf{B} = \begin{pmatrix} 1 & 0 & 0 \\ 0 & 1 & 0 \\ 0 & 0 & 1 \end{pmatrix},$$

$$\mathbf{C} = \begin{pmatrix} a_1 & b_1\Delta x & c_1(\Delta x)^2 \\ \frac{a_2}{\Delta x} & b_2 & c_2\Delta x \\ \frac{a_3}{(\Delta x)^2} & \frac{b_3}{\Delta x} & c_3 \end{pmatrix}, \quad \mathbf{O} = \begin{pmatrix} 0 & 0 & 0 \\ 0 & 0 & 0 \\ 0 & 0 & 0 \end{pmatrix}, \tag{2.21}$$

$$\mathbf{x}_i = \begin{pmatrix} f_i' \\ f_i'' \\ f_i''' \end{pmatrix}, \text{ and } \quad \mathbf{d}_i = \begin{pmatrix} \frac{d_1}{\Delta x}(f_{i+1} - f_{i-1}) \\ \frac{d_2}{(\Delta x)^2}(f_{i+1} - 2f_i + f_{i-1}) \\ \frac{d_3}{(\Delta x)^3}(f_{i+1} - f_{i-1}) \end{pmatrix}.$$

The operation count for this scheme is proportional to N, which is the same order as the ordinary difference scheme.

3. Solution method

Williamson's standard test suites [19] are used for performance measurement of the sp-CCD scheme.

3.1. Governing equations

The shallow water equations on a sphere whose radius is a can be written in advective form as

$$\frac{\partial u}{\partial t} + \mathbf{v}\cdot\nabla u - \left(f + \frac{u}{a}\tan\theta\right)v + \frac{g}{a\cos\theta}\frac{\partial h}{\partial \lambda} = 0, \tag{3.22}$$

$$\frac{\partial v}{\partial t} + \mathbf{v}\cdot\nabla v + \left(f + \frac{u}{a}\tan\theta\right)u + \frac{g}{a}\frac{\partial h}{\partial \theta} = 0, \tag{3.23}$$

and

$$\frac{\partial h^*}{\partial t} + \mathbf{v}\cdot\nabla h^* + \frac{h^*}{a\cos\theta}\left(\frac{\partial u}{\partial \lambda} + \frac{\partial v\cos\theta}{\partial \theta}\right) = 0, \tag{3.24}$$

where h^* is the depth of the fluid and h is the height of the free surface above a reference sphere. $h = h^* + h_s$ where h_s is the height of the underlying topography. Here $\mathbf{v}$ is the horizontal vector velocity of the fluid with components u and v in the longitudinal (λ) and latitudinal (θ) directions, respectively, g the gravitational constant, f the Coriolis parameter given by $2\Omega\sin\theta$, where Ω is the rotation rate of the sphere, and the longitudinal, latitudinal, and outward radial unit vectors are $\hat{\mathbf{i}}$, $\hat{\mathbf{j}}$, and $\hat{\mathbf{k}}$, respectively. The ∇ operator is the spherical horizontal gradient operator given by

$$\nabla(\bullet) \equiv \frac{\hat{\mathbf{i}}}{a\cos\theta}\frac{\partial}{\partial\lambda}(\bullet) + \frac{\hat{\mathbf{j}}}{a}\frac{\partial}{\partial\theta}(\bullet). \tag{3.25}$$

The relative vorticity ζ and horizontal divergence δ are defined by

$$\zeta \equiv \hat{\mathbf{k}}\cdot(\nabla\times\mathbf{v}) = \frac{1}{a\cos\theta}\left(\frac{\partial v}{\partial\lambda} - \frac{\partial u\cos\theta}{\partial\theta}\right), \tag{3.26}$$

and

$$\delta \equiv \nabla\cdot\mathbf{v} = \frac{1}{a\cos\theta}\left(\frac{\partial u}{\partial\lambda} + \frac{\partial v\cos\theta}{\partial\theta}\right), \tag{3.27}$$

respectively.

3.2. Numerical method

3.2.1. Grid system

The longitude-latitude grid system used by Fornberg [5] was utilized for computation. The grid points in this system are arranged so that no grid points are at the poles. This grid system has the advantage of avoiding singularity at the poles and enabling the periodic boundary conditions to be imposed in both longitudinal and latitudinal direction. Fig. 3 illustrates how the periodic boundary conditions can be imposed in latitudinal direction. It should be noted that the sign of the quantities must be adjusted properly when using the periodic boundary condition in latitudinal direction, depending on whether the quantities are scalar or vector. The spatial derivatives of each physical quantity in the shallow water equations were calculated by sp-CCD scheme and the time integration was done by the fourth-order Runge–Kutta method. The stability limit of the scheme is given by $c\Delta t/\Delta x \leqslant 1.06$ in the one-dimensional problem, where c is the advective velocity, Δt the time step, and Δx the grid spacing.

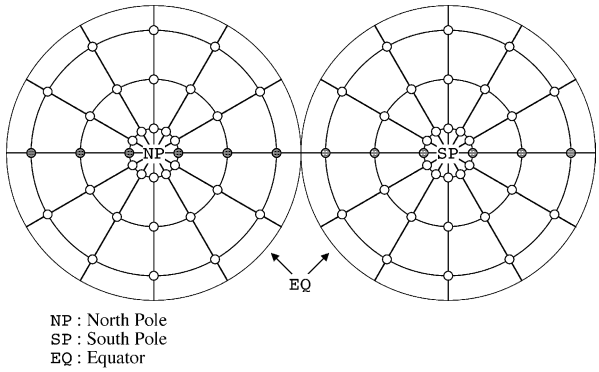

Fig. 3. The longitude–latitude grid system used in this paper. The latitude grid points are shifted a half-grid length. The periodic boundary conditions can be applied for the latitudinal direction.

3.2.2. Low-pass spatial filter

The concentration of the grid points near the poles causes numerical instability. A spatial filter is used to remove this instability. In the Appendix of [10], Lele proposed a pentadiagonal implicit spatial filter in the form of

$$\overline{f}_i + \alpha\left(\overline{f}_{i+1} + \overline{f}_{i-1}\right) + \beta\left(\overline{f}_{i+2} + \overline{f}_{i-2}\right) = af_i + \frac{b}{2}(f_{i+1} + f_{i-1}) + \frac{c}{2}(f_{i+2} + f_{i-2}) + \frac{d}{2}(f_{i+3} + f_{i-3}), \tag{3.28}$$

where $\overline{f}_i$ is the filtered value at grid point x_i. The Fourier analysis of (3.28) gives the transfer function

$$T(w) = \frac{a + b\cos(w) + c\cos(2w) + d\cos(3w)}{1 + 2\alpha\cos(w) + 2\beta\cos(2w)}. \tag{3.29}$$

There are six parameters of a, b, c, d, α, and β. Lele proposed a way of determining those parameters in order to adjust the location of cutoff in the transfer function [10]. He required a formal fourth-order accuracy in (3.28), i.e.,

$$T(0) = 1, \frac{\mathrm{d}^2 T}{\mathrm{d}w^2}(0) = 0, \tag{3.30}$$

and

$$T(\pi) = 0, \frac{\mathrm{d}^2 T}{\mathrm{d}w^2}(\pi) = 0, \tag{3.31}$$

and

$$T(w_1) = v_1, T(w_2) = v_2, \tag{3.32}$$

where w_1, w_2, v_1, and v_2 are specified to determine the cutoff wavenumber of the filtering. However, the obtained filter is not necessarily valid. That is, the transfer function may have the overshoot ($T(w) > 1$) and/or the undershoot ($T(w) < 0$) depending on the combination of the values of w_1, w_2, v_1, and v_2. It is difficult to show the condition of overshooting and/or undershooting for given w_1, w_2, v_1, and v_2. Therefore, applying this way of determining parameters is troublesome because of the filtering of small scales near the poles. Therefore another way of determining the parameters is desired. We determined those parameters by using the constraints instead of (3.32),

$$T(w_c) = \frac{1}{2}, \tag{3.33}$$

and

$$0 < T(w) < 1 \quad \text{for } 0 < w < \pi, \tag{3.34}$$

and requiring the filter should have sharp cutoff property as far as possible. Here w_c $(0 < w_c < \pi)$ is specified to determine the critical wavenumber of the filtering. By this way, the parameters are determined as

$$\begin{aligned}
\beta &= \min\left(\frac{4 - 3\cos w_c + 2\cos^2 w_c + \cos^3 w_c}{16 - 2\cos w_c + 4\cos^2 w_c + 6\cos^3 w_c}, \frac{3 + 3\cos w_c + 3\cos^2 w_c - \cos^3 w_c}{10 + 2\cos w_c + 10\cos^2 w_c - 6\cos^3 w_c}\right), \\
\alpha &= \frac{\cos w_c}{2(1 + \cos^2 w_c)}\left\{2\beta - 3 + (1 - 6\beta)\cos^2 c_w\right\}, \\
a &= \frac{3\alpha + 2}{4}, \quad b = \frac{16\alpha + 10\beta + 9}{16}, \quad c = \frac{\alpha + 4\beta}{4}, \quad d = \frac{6\beta - 1}{16}.
\end{aligned} \tag{3.35}$$

Fig. 4 shows the transfer function for our filtering scheme with various w_c. In this study, w_c is chosen as

$$w_c = \begin{cases} w_{\max}\{1 - 0.75(1 - \cos\theta)^5\} & \text{(for longitudinal direction)}, \\ w_{\max} & \text{(for latitudinal direction)}, \end{cases} \tag{3.36}$$

where $w_{\max}$ is set to $w_{\max} = 0.952\pi$. This filtering scheme is a pentadiagonal system and solved with the cost of proportional to N. Shang [16] proposed a tridiagonal implicit spatial filter scheme in CEM problem. By changing parameters, the property of the filter can be controlled. It is, however, not enough for our purpose where most of the waves should be filtered out. In comparison with the case where the filter proposed by Shang is applied, the calculation with our filter is more stable and the results are more accurate. The l_2 error for the Test Case 1 (see Section 4) with our filter, for example, is about a half of that in [18]. The filtering is applied to the variable of u, v, and h in shallow water Eqs. (3.22)–(3.24) for each time step and each step of

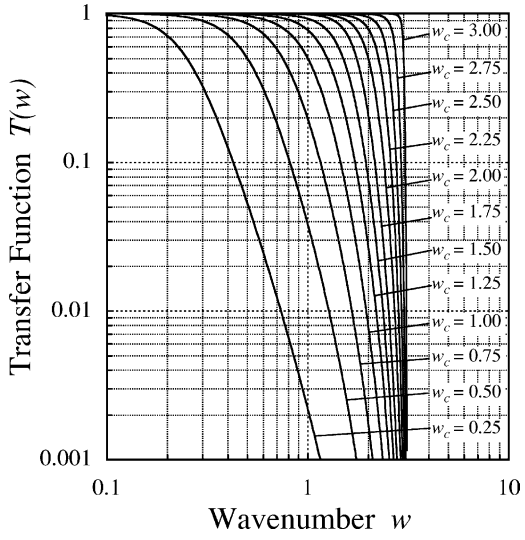

Fig. 4. Transfer functions T for the compact filter scheme with various parameter values.

the Runge–Kutta method. It is noted that we applied filtering to h, not to h^*, to prevent spurious smoothing associated with the surface topography.

4. Results

The standard test set proposed by Williamson et al. [19] consists of seven test cases. Detailed mathematical formulas of the test cases and requested performance measurements are intensively described in [19]. Test Cases 1–4 have analytic solutions. Since Test Cases 5–7 have no analytic solutions, numerical solutions of high-resolution spherical harmonics model are regarded as true solutions in error measurements. A T341 model which has the grid numbers of 1024×512 is used to generate reference solutions in this study. The spherical harmonics model was coded by using the subroutine library for scientific computing 'ispack' [7]. The following normalized global errors are used for error measurements in all test cases

$$l_1(q) = \frac{I[|q(\lambda,\theta) - q_{\mathrm{T}}(\lambda,\theta)|]}{I[|q_{\mathrm{T}}(\lambda,\theta)|]}, \tag{4.37}$$

$$l_2(q) = \frac{\left(I\left[|q(\lambda,\theta) - q_{\mathrm{T}}(\lambda,\theta)|^2\right]\right)^{1/2}}{\left(I\left[|q_{\mathrm{T}}(\lambda,\theta)|^2\right]\right)^{1/2}}, \tag{4.38}$$

$$l_\infty(q) = \frac{\max_{\mathrm{all}}\,\lambda,\theta|q(\lambda,\theta) - q_{\mathrm{T}}(\lambda,\theta)|}{\max_{\mathrm{all}}\,\lambda,\theta|q_{\mathrm{T}}(\lambda,\theta)|}, \tag{4.39}$$

where q and q_{T} are physical quantity of the numerical solution and the true solution, respectively, and $I[\bullet]$ is a discrete approximation to the global integral

$$I_c[q] = \frac{1}{4\pi}\int_0^{2\pi}\int_{-\pi/2}^{\pi/2} q(\lambda,\theta)\cos\theta\,\mathrm{d}\theta\,\mathrm{d}\lambda, \tag{4.40}$$

which gives the global mean of a physical quantity.

In this study, $I[\bullet]$ is defined as

$$I[q] = \frac{1}{4\pi}\sum_{k=1}^{N_\lambda}\sum_{l=1}^{N_\theta} q_{k,l}\cos\theta_l \cdot 2\sin(\Delta\theta/2)\Delta\lambda, \tag{4.41}$$

where N_λ and N_θ are the number of grid points in longitudinal and latitudinal direction, $\Delta\lambda = 2\pi/N_\lambda$, $\Delta\theta = \pi/N_\theta$, and $q_{k,l}$ is a physical quantity at the grid point of $(\lambda,\theta) = (\lambda_k,\theta_l) = (-\pi + k\Delta\lambda, -\pi/2 + (l-1/2)\Delta\theta)$, respectively. This is defined in order that $I[\bullet]$ satisfies $I[\overline{q}] = \overline{q}$ independently of the grid resolution when $\overline{q}$ is constant.

In this study, the calculation was performed in double precision format and with the grid numbers of 128×64 ($N_\lambda = 128$ and $N_\theta = 64$) unless mentioned otherwise.

4.1. Test Case 1 – advection of cosine bell over the pole

Test Case 1 is the test for the advective component of a numerical scheme. For this test case, a cosine bell is advected once around the sphere by the flow of solid body rotation. The parameter α is used to set the direction of the flow so that the cosine bell will be advected directly around the equator ($\alpha = 0$), directly

over the poles ($\alpha = \pi/2$), and at slight angles (0.05 radians) to these extremes, to check the effects of asymmetries and the 'polar problem'.

The calculation was done with the time step of 576 s. The height field after one rotation for the case of $\alpha = \pi/2 - 0.05$ is shown in Fig. 5. Though the initial height field is also plotted in Fig. 5 with dashes, it is almost indistinguishable from the final height field. The error field shown in Fig. 6 has a nearly concentric circular structure with alternating sign having the maximum amplitude near the edge of the cosine bell. This

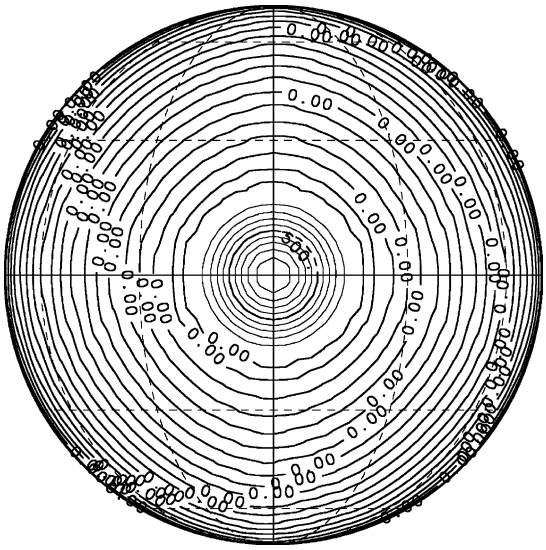

Fig. 5. Height field after one rotation for Test Case 1 with $\alpha = \pi/2 - 0.05$. The contour interval is 100 m.

Fig. 6. Height error after one rotation for Test Case 1 with $\alpha = \pi/2 - 0.05$. The contour interval is 1.25 m. Negative regions are shaded.

structure is due to the initial discontinuity of the second and higher order derivative of the cosine bell at its edge. The fact that only a little distortion can be seen in the structure indicates accuracy of dispersion relation for wide range of wavenumbers in our scheme. That is, not only the cosine bell, the advection of that structure which has relatively short scale variation is also properly handled by our scheme. It should be noted that the maximum amplitude of that error field is as small as 0.3% of the height of the cosine bell. For the other cases, the results are quite similar to the case described above.

Table 1 shows the values of $l_1(h)$, $l_2(h)$, and $l_\infty(h)$ errors after one rotation for various schemes, where the values for the double Fourier method are read from Fig. 9(a) of [2]. It indicates that the compact difference schemes have much higher accuracy than the ordinary central difference schemes and that the spectral-like schemes (sp-CD4 and sp-CCD8) are more accurate than ordinary schemes. It is concluded that these results directly reflect the resolution of the scheme on the sphere. The $l_2(h)$ error of the sp-CCD scheme is about 10 times larger than that of the spherical harmonics method. The errors of the double Fourier method are larger than those of sp-CCD, however, it should be considered that the time integration scheme might be different from that used in this study. The $l_2(h)$ error of the method of Spotz et al. [17] is about 10 times larger than that of sp-CCD method. The $l_2(h)$ error of spherical harmonics method calculated by them [17] is also larger than that calculated by us. They used a leapfrog method for the time integration.

The time evolution of the normalized mean

$$M = (I[h] - I[h_T])/I[h_0], \tag{4.42}$$

the variance

$$V = \{I[(h - I[h])^2] - I[(h_T - I[h_T])^2]\}/I[(h_0 - I[h_0])^2], \tag{4.43}$$

the maximum

$$h_{\max} = \left(\max_{\text{all}\lambda,\theta} h(\lambda,\theta) - \max_{\text{all}\lambda,\theta} h_T(\lambda,\theta) \right) \Big/ \Delta h, \tag{4.44}$$

and the minimum [19]

Table 1
$l_1(h)$, $l_2(ht)$, and $l_\infty(h)$ errors for Tast Case 1 after one rotation with grid resolution of 128×64 for various schemes ($\alpha = \pi/2 - 0.05$)

Scheme	$l_1(h)$	$l_2(h)$	$l_\infty(h)$
FD2	1.9396	0.7456	0.5932
FD4	0.3570	0.1172	0.0798
FD6	0.1544	0.0414	0.0344
FD8	0.0904	0.0222	0.0128
sp-CD4	0.0080	0.0042	0.0038
CCD6	0.0348	0.0102	0.0070
CCD8	0.0158	0.0058	0.0048
sp-CCD8	0.0074	0.0038	0.0028
SH	0.0004	0.0002	0.0004
DF	0.047	0.014	0.012
COM4/SHF	N/A	0.042	N/A

(FD2) second-order central differences; (FD4) fourth-order central differences; (FD6) sixth-order central differences; (FD8) eighth-order central differences; (sp-CD4) spectral-like fourth-order compact difference scheme; (CCD6) sixth-order combined compact difference scheme; (CCD8) eighth-order combined compact difference scheme; (sp-CCD8) new spectral-like eighth-order combined compact difference scheme; (SH) spectral transform method using spherical harmonics; (DF) spectral transform method using double Fourier series read from Fig. 9(a) of [3]; (COM4/SHF) fourth-order compact difference scheme with the spherical harmonic filter taken from Table II of [17].

$$h_{\min} = \left(\min_{\text{all}\lambda,\theta} h(\lambda,\theta) - \min_{\text{all}\lambda,\theta} h_T(\lambda,\theta) \right) \Big/ \Delta h \tag{4.45}$$

are calculated for error measurement. Here h_0 is the initial field and Δh is the difference between the maximum and minimum values of the true initial solution. The time evolution of the normalized mean is averagely flat. It shows that the total mass is conserved well during the calculation. The small values of the variance and the maximum, which are of the order of 10^{-4} and 10^{-5}, respectively, show that the distortion and damping of the cosine bell is sufficiently small. The small value of the minimum which is of the order of 10^{-4} shows that the amplitude of the concentric structure around the cosine bell is small, and its time evolution indicates that the growth of the amplitude tends to slow down. These tendency are also similar for all cases of α.

4.2. Test Case 2 – global steady-state nonlinear zonal geostrophic flow

Test Case 2 is the test for the hold of a steady-state solution to the nonlinear shallow water equations. The initial condition that should be kept through time integration consists of solid body rotational flow with the corresponding geostrophic height field. The parameter α is also used in this test case, which is the angle between the axis of the computational grid and the axis about which geostrophic flow take place. In this system, the numerical error can propagate as gravity wave with the velocity that is much greater than that of the flow. Therefore, for the purely explicit scheme, the time step restricted by the CFL condition is almost determined by the speed of the gravity wave and the longitudinal grid spacing near the poles.

Williamson et al. [19] recommended to modify the initial wind and height fields so they satisfy a discrete nonlinear geostrophic relationship consistent with the scheme. In this study, however, no modification was made on the initial fields. The calculation was done with the time step of 30 s. The height field (not shown) is almost indistinguishable from the initial height field. The strong flow passes the polar region for this case, however, no significant error can be seen in the height field, which is at most 0.16 m. The error of $\mathbf{v}$ is about 10 times larger than that of h. The fluctuation due to the gravity wave can be seen in l_∞ error of h. Fig. 7 shows $l_2(h)$ and $l_2(\mathbf{v})$ errors for different resolutions in the case of $\alpha = \pi/2 - 0.05$ at Day 5. In this case, the time step is set to 2.5 s for all resolutions. The rate of convergence may be estimated as fourth order. This corresponds to the accuracy of the fourth-order spatial filer. The error for the spectral method is of the order of rounding error [3] or 10^{-10} [8] because the method uses vorticity–divergence form or stream function, velocity potential form in which one of the variables vanishes in this case. The error for the method of Spotz et al. [17] is also small, which is of the order of 10^{-8} because the method uses vector invariant form and the divergence of the velocity field vanishes in this case.

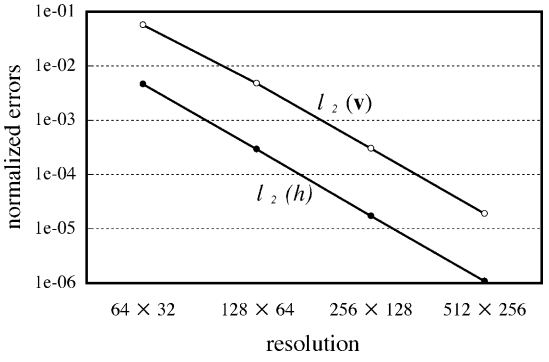

Fig. 7. l_2 errors at day 5 versus model resolution for Test Case 2, $\alpha = \pi/2 - 0.05$.

4.3. Test Case 3 – steady-state nonlinear zonal geostrophic flow with compact support

Test Case 3 is similar to the Test Case 2 except that the initial wind field is nonzero in a limited region. In this test case, some integration is needed to obtain the initial height field from the initial wind field. In this study, that integration was done numerically by the Simpson's formula with sufficient division of the integral range to converge within the order of 10^{12} in term of the relative error. In the case of $\alpha = \pi/3$, the strong flow passes the polar region, so this case is harsh to our scheme.

The calculation was done with the time step of 30 s. The height field (not shown) is indistinguishable from the initial height field and no significant error can be seen. The amplitude of these errors is as small as that of the Test Case 2 since there is no essential differences between Test Case 2 and 3 for our scheme. The height error, however, localizes in downstream of the pole whereas the error for the Test Case 2 is located away from the poles. The error for the spectral method is very small, which is of the order of 10^{-8} [3] or 10^{-10} [8], for the same reason for the Test Case 2.

4.4. Test Case 4 – forced nonlinear system with a translating low

Test Case 4 is the forced nonlinear system with translating low superimposed on a jet stream that is symmetrical about the equator. The parameter u_0 is used in this test case to specify the intensity of the jet. The forcing term is defined using temporal differentiation, spatial differentiation, and spatial integration. In this study, the forcing term is calculated analytically.

The calculation was done with $u_0 = 20$ and $u_0 = 40$ m/s. The time step is set to 60 s in both cases. Contour maps of height field and its error after 5 days for $u_0 = 40$ are shown in Figs. 8 and 9, respectively. The height field shown in Fig. 8 is indistinguishable from initial condition (not shown). The largest error appears in the vicinity of the translating low. This behavior is similar to that of the spectral method [3,8]. In this case, l_1, l_2, and l_∞ errors of $\mathbf{v}$ are about the same order of amplitude as those of h. The l_2 height errors are smaller than those of the spectral method [3,8]. The difference of the amplitude of l_2 height error between the case of $u_0 = 20$ m/s and the case of $u_0 = 40$ m/s is also smaller than that of the

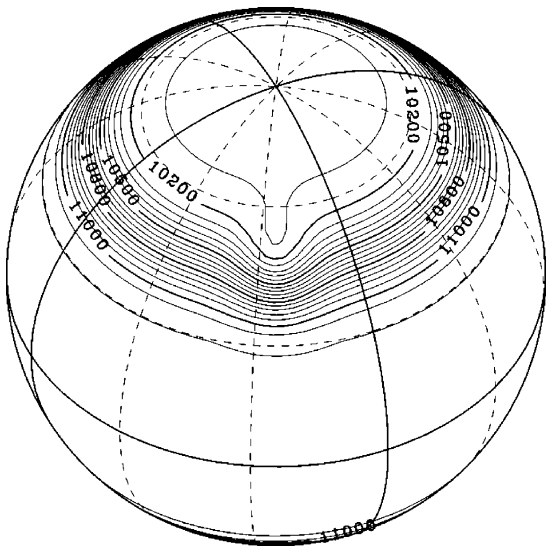

Fig. 8. Height field at Day 5 for Test Case 4 with $u_0 = 40$ m/s.

Fig. 9. Height error at Day 5 for Test Case 4 with $u_0 = 40$ m/s. The contour interval is 0.2 m. Negative regions are shaded.

spectral method [3,8]. It should be noted that the time integration scheme might be different from that used in this study.

4.5. Test Case 5 – zonal flow over an isolated mountain

Test Case 5 consists of the solid body rotational flow similar to that of the Test Case 2 with $\alpha = 0$ impinging on a mountain. The mountain is located at (30°N, 90°W) and has the shape of a cone. Since the geostrophic balance is broken at the beginning of the calculation due to the existence of the mountain, the gravity wave arises and spreads all over the sphere. This can be the source of error together with the discontinuity of the gradient of the mountain.

The calculation was done with time step of 60 s. The height field and its error after 15 days are shown in Figs. 10 and 11, respectively. The height field shown in Fig. 10 is indistinguishable from the reference

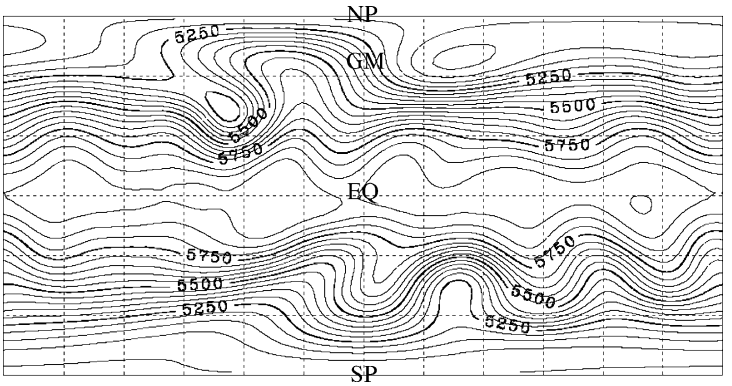

Fig. 10. Height field at Day 15 for Test Case 5. The contour interval is 50 m.

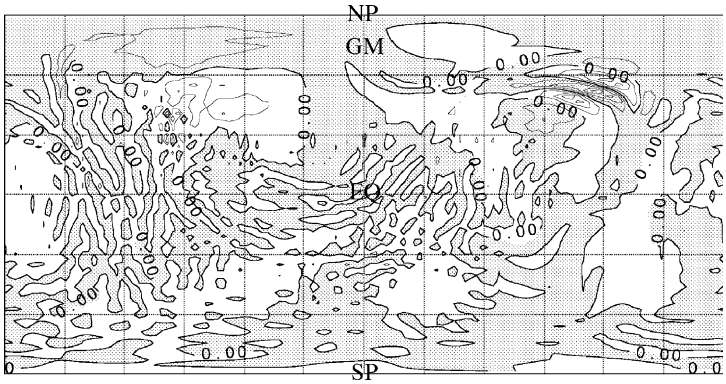

Fig. 11. Height error at Day 15 for Test Case 5. The contour interval is 0.5 m.

solution (not shown). Fig. 11 shows that the error due to the gravity wave spreads over the sphere. The errors of $\mathbf{v}$ are about 10 times larger than those of h. The l_2 height error is smaller than that of the spectral method [3,8]. In this study, we use the T341 reference solution while the T213 solution is used in [3,8]. But this does not cause significant difference in the error measurement. The mass, the energy, and the potential enstrophy conserve almost in the same order (see Table 3). Although the mass conservation is worse than that of spectral method, each conservation property is considered to be good enough for practical use. The error of the total energy is smaller than that of the spectral method using the double Fourier series [3].

4.6. Test Case 6 – Rossby–Haurwitz wave

Test Case 6 is the Rossby–Haurwitz wave of the zonal wavenumber 4. It is the exact analytical solution of the nonlinear nondivergent barotropic vorticity equation that translates zonally with the shape preserved. It is, however, not the solution to the shallow water equations, so the shape is not maintained. The calculation was done with time step of 60 s. The height field and its error after 14 days are shown in Figs. 12 and 13, respectively. The height field shown in Fig. 12 is almost indistinguishable from reference solution (not shown). Fig. 13 shows that the error related with the location of the wave is considerably small. It indicates the high accuracy of our scheme in calculation of the phase speed of the wave. The errors of $\mathbf{v}$ are also about 10 times larger than those of h. The l_2 height error is a little bit larger than that of the spectral method using the double Fourier series [3]. The error becomes large in the polar region due to the spatial

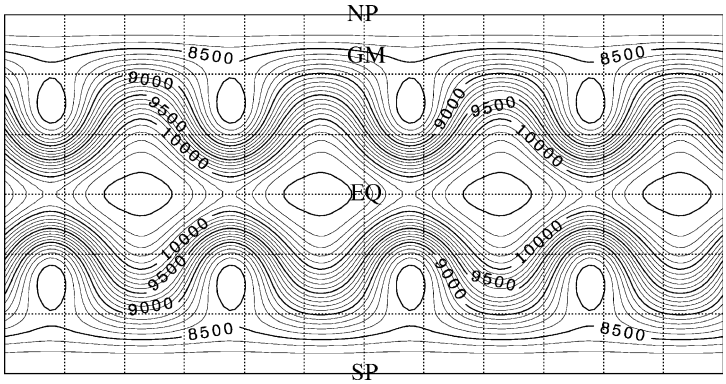

Fig. 12. Height field at Day 14 for Test Case 6. The contour interval is 100 m.

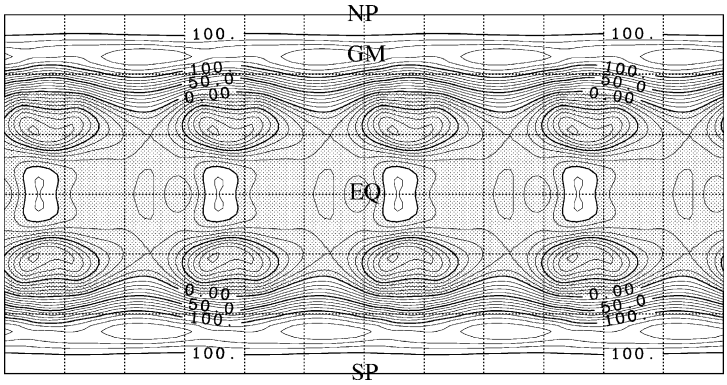

Fig. 13. Height error at Day 14 for Test Case 6. The contour interval is 10 m. Negative regions are shaded.

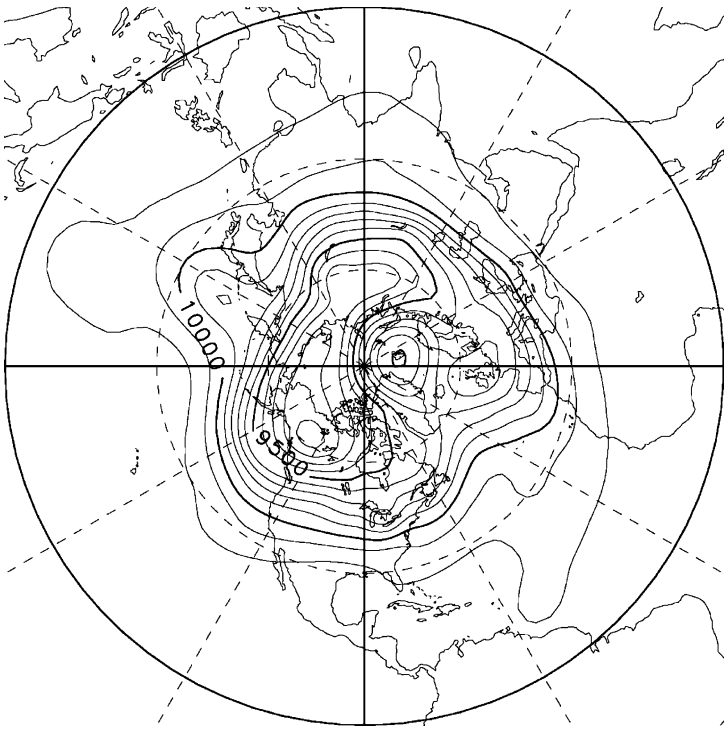

Fig. 14. Height field at Day 5 for Test Case 7 of the 21 December 1978. The contour interval is 100 m.

filter. Although the conservation of potential enstrophy is a little bit worse than that of the others, each value is considered to be good enough for practical use. The error of the total energy is smaller than that of the spectral method [3,8].

4.7. Test Case 7 – analyzed 500 mb height and wind field initial conditions

Test Case 7 uses the analyzed 500 mb height and wind field as initial conditions. Since the observed data was obtained as spectral coefficient, the Legendre transform was used to generate the initial values at the

grid points of our scheme. In this study, no further data processing such as nonlinear normal mode initialization was performed.

The calculation was done with the time step of 60 s. The height field and its error after five days for the case of 0000 GMT December 21, 1978 are shown in Figs. 14 and 15, respectively. The height field shown in Fig. 14 is quite similar to the reference solution (not shown). Fig. 15 shows that the errors in the small scales

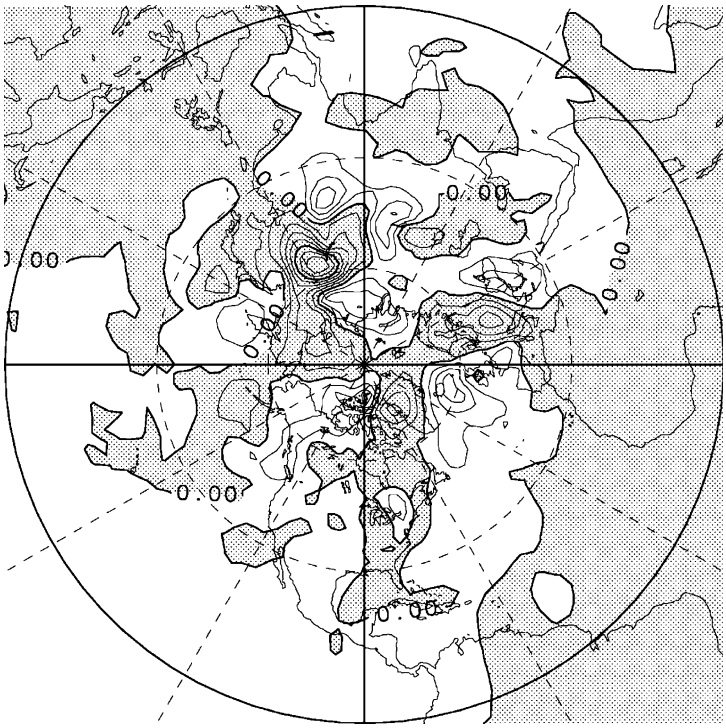

Fig. 15. Height error at Day 5 for Test Case 7 of the 21 December 1978. The contour interval is 25 m. Negative regions are shaded.

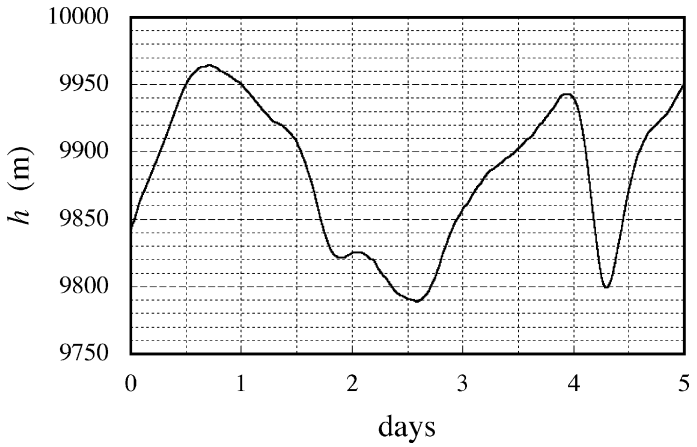

Fig. 16. Height field as a function of time at grid points closest to (40°N, 105°W) for Test Case 7.

are dominant. In this case, the errors of $\mathbf{v}$ are about 100 times larger than those of h. The l_2 height error is smaller than that of the spectral method [3]. Although the conservation of potential enstrophy is a little bit worse than that of the others, each value is considered to be good enough for practical use. Fig. 16 shows the trace of the height field at the grid point closest to (40°N, 105°W) for the case of 0000 GMT December 21, 1978. No significant oscillation due to gravity wave is present.

5. Discussion and conclusions

Application to the standard test set for the shallow water equations shows the high accuracy and resolution of the spectral-like CCD scheme described in Section 2. Results of the error measurements for all test cases are summarized in Tables 2 and 3. In the case 1 of a linear problem, the accuracy is better than that of original CCD scheme, and is much better than those of the ordinary central difference schemes. In this paper, we use the fourth-order Runge–Kutta scheme for the time integration. However, the time integration scheme used in the double Fourier method by Cheong [2] is not clear. Spotz et al used a leapfrog time integration [17], but the errors of their spherical harmonics method are smaller than those of Jakob-Chien et al. [8] who also used a spectral method with leapfrog time integration. The errors of the spherical harmonics method used in this paper are also much smaller than that reported in [17]. These indicate that the relationship between the time integration scheme and the spatial scheme are not negligible in comparison. Therefore it is difficult to make direct comparison of our method with others. However, the errors of our method are of the similar magnitude for all of the test cases, and for the nonlinear, unsteady cases 5, 6, and 7, they are similar to, or even less than those of the other methods [3,8,17].

A spatial filtering scheme is improved so that the cutoff wavenumber is easily specified. This filter acts not only as the smoother to avoid the polar problem but also the hyper viscosity to eliminate the aliasing error of the nonlinear advection terms. By using this filter, the CFL condition is relaxed, so that the stable calculations can be performed with the time step that is up to about twice as large as that obtained from the CFL condition estimated in Section 3.

Table 2
The error measurements after the specified time for each test case

Test Case	$l_1(h)$	$l_2(h)$	$l_\infty(h)$	$l_1(\mathbf{v})$	$l_2(\mathbf{v})$	$l_\infty(\mathbf{v})$
1 ($\alpha = \pi/2 - 0.05$)	7.4×10^{-3}	3.8×10^{-3}	2.8×10^{-3}	–	–	–
2 ($\alpha = \pi/2 - 0.05$)	1.8×10^{-5}	2.4×10^{-5}	5.2×10^{-5}	2.5×10^{-4}	3.9×10^{-4}	2.1×10^{-3}
3 ($\alpha = \pi/3$)	7.4×10^{-6}	1.6×10^{-5}	1.2×10^{-4}	3.4×10^{-4}	5.8×10^{-4}	2.5×10^{-3}
4 ($u_0 = 20$)	2.1×10^{-3}	7.1×10^{-4}	1.1×10^{-3}	3.0×10^{-3}	1.1×10^{-3}	1.8×10^{-3}
4 ($u_0 = 40$)	3.8×10^{-3}	8.7×10^{-4}	1.0×10^{-3}	5.2×10^{-3}	1.3×10^{-3}	1.4×10^{-3}
5	2.3×10^{-5}	4.0×10^{-5}	3.5×10^{-4}	1.6×10^{-3}	3.2×10^{-3}	1.6×10^{-2}
6	4.0×10^{-3}	5.8×10^{-3}	1.3×10^{-2}	6.2×10^{-2}	6.8×10^{-2}	7.5×10^{-2}
7	9.7×10^{-4}	1.8×10^{-3}	1.9×10^{-2}	1.8×10^{-1}	2.2×10^{-1}	5.6×10^{-1}

Table 3
The error measurements of the global invariants for Test Cases 5–7

Test Case	Mass	Energy	Potential enstrophy	Vorticity	Divergence
5	1.8×10^{-6}	3.1×10^{-6}	-2.3×10^{-5}	-1.3×10^{-9}	-5.1×10^{-11}
6	2.1×10^{-6}	2.1×10^{-6}	-1.0×10^{-3}	2.2×10^{-17}	-1.1×10^{-9}
7	1.1×10^{-6}	-4.1×10^{-5}	-4.3×10^{-2}	-1.2×10^{-8}	7.5×10^{-11}

Since both the CCD scheme and the spatial filtering scheme have the same order of operation count $O(N)$ in the one-dimensional calculation with N grid points, the total operation count for our method is proportional to the total number of grid points, i.e., $O(N^2)$. Therefore this method is the fastest in terms of the order of the operation count and is advantageous in solving large systems. The computational time for one time step using 1PE of Fujitsu VPP-5000 is shown in Fig. 17. It exhibits this low growth of the computational cost. The spherical harmonics model (SH) [7] is also shown in Fig. 17. This spherical harmonics model is optimized for this vector machine. The time required for our model becomes smaller than that of the spherical harmonics model for the grid resolution of 512×256, and the difference becomes greater for higher resolutions.

There are at least four problems that remain to be studied in the future:

(1) We used a full explicit scheme, which restricts the time step to short interval given by the CFL condition. Though this restriction is relaxed somewhat by the spatial filter, it increases the total amount of calculation for the time integration of the given duration. Some semi-implicit scheme and/or some grid system other than the longitude–latitude grid should be studied for the practical problem.

(2) In this paper, we use the advective form of the shallow water equations considering the application to the general problem. However, this discrete expression gives no guarantee for the conservation of any invariants. The property of conservation can be improved by using the conservative forms such as the flux form that ensures the conservation of mass.

(3) The parameters of the spatial filter are fixed in this study. It should be noted that the effect of spatial filter in our method becomes stronger as the time step becomes shorter without changing the parameters of the filter. This feature makes the calculation at high resolution more stable. However, too short time step causes unnecessary damping. In general, preferable result was obtained for the long time step as possible. But, at present, the relationship between the adequate time step and filtering is unclear.

(4) The spectral-like CCD scheme can be applied to problems that have boundary such as ocean circulation model and regional climate model. The treatment of the boundary is described in [4]. The formal

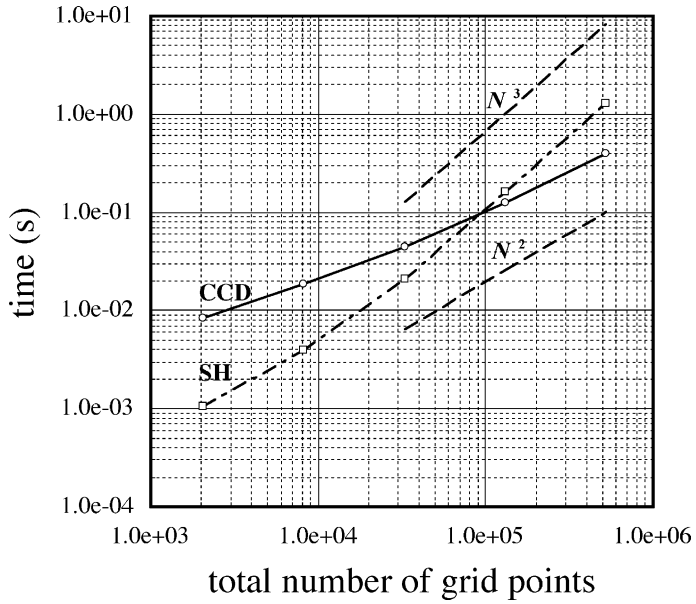

Fig. 17. The computational time for one time step calculation of Test Case 2 with $\alpha = \pi/4$.

accuracy degrades at the boundary. The resolution characteristics of the boundary scheme is remained for the future study. For one-dimensional problems, Kobayashi [9] studied the boundary effects on the global accuracy and the stability in the case of finite volume method. Similer study is need for the CCD scheme. The effects of boundary for two-dimensional and three-dimensional problems should be studied for these applications.

Finally, the test results presented in this study show that our method is thought to be promising for a variety of numerical models including high-resolution models for weather prediction.

Acknowledgements

We thank Dr. Koji Akahori for providing the spectral transform solutions to the Williamson's test cases and for many fruitful discussions. We also thank Satoshi Sugiura for many discussions on the speedup of our codes. The authors are grateful to Prof. Yukio Kaneda and Dr. Takashi Ishihara for many useful remarks on this study. We are thankful to Teppei Hojo for his comments on a draft of this paper. Some figures were produced by GFD-DENNOU Library. The authors appreciate that GFD-DENNOU Club distributes such a useful and portable library. Computer resources were provided by the Information Technology Center of Nagoya University. This study was supported by "Research for the Future" Program of the Japan Society for the Promotion of Science under the project JSPS-RFTF97P01101.

References

[1] N.A. Adams, K. Shariff, A high-resolution hybrid compact-ENO scheme for shock–turbulence interaction problems, J. Comput. Phys. 127 (1996) 27.
[2] H.-B. Cheong, Double Fourier series on a sphere: applications to elliptic and vorticity equations, J. Comput. Phys. 157 (2000) 327.
[3] H.-B. Cheong, Application of double Fourier series to the shallow-water equations on a sphere, J. Comput. Phys. 165 (2000) 261.
[4] P.C. Chu, C. Fan, A three-point combined compact difference scheme, J. Comput. Phys. 140 (1998) 370.
[5] B. Fornberg, A pseudospectral approach for polar and spherical geometries, SIAM J. Sci. Comput. 16 (5) (1995) 1071.
[6] R. Hixon, Prefactored small-stencil compact schemes, J. Comput. Phys. 165 (2000) 522.
[7] K. Ishioka, ispack-0.5, GFD Dennou Club, 2000. Available from <http://www.gfd-dennou.org/arch/ispack/>.
[8] R. Jakob-Chien, J.J. Hack, D.L. Williamson, Spectral transform solutions to the shallow water test set, J. Comput. Phys. 119 (1995) 164.
[9] M.H. Kobayashi, On a class of Padé finite volume methods, J. Comput. Phys. 156 (1999) 137.
[10] S.K. Lele, Compact finite difference schemes with spectral-like resolution, J. Comput. Phys. 103 (1992) 16.
[11] S.-J. Lin, R.B. Rood, An explicit flux-form semi-Lagrangian shallow-water model on the sphere, Quart. J. R. Meteorol. Soc. 123 (1997) 2477.
[12] K. Mahesh, A family of high order finite difference schemes with good spectral resolution, J. Comput. Phys. 145 (1998) 332.
[13] H.L. Meitz, H.F. Fasel, A compact-difference scheme for the Navier–Stokes equations in vorticity–velocity formulation, J. Comput. Phys. 157 (2000) 371.
[14] P.E. Merilees, The pseudospectral approximation applied to the shallow water equations on a sphere, Atmosphere 11 (1973) 13.
[15] M. Rančić, R.J. Purser, F. Mesinger, A global shallow-water model using an expanded spherical cube: genomic versus conformal coordinates, Quart. J. R. Meteorol. Soc. 122 (1996) 959.
[16] J.S. Shang, High-order compact-difference schemes for time-dependent Maxwell equations, J. Comput. Phys. 153 (1999) 312.
[17] W.F. Spotz, M.A. Taylor, P.N. Swarztrauber, Fast shallow-water equation solvers in latitude–longitude coordinates, J. Comput. Phys. 145 (1998) 432.
[18] S. Sugiura, Fluid calculation on a sphere using combined compact scheme, Master Thesis, Nagoya University, 2000 (in Japanese).
[19] D.L. Williamson, J.B. Drake, J.J. Hack, R. Jakob-Chien, P.N. Swarztrauber, A standard test set for numerical approximations to the shallow water equations in spherical geometry, J. Comput. Phys. 102 (1992) 211.